Overview of the Experimental and Analytical Results for the HDR-RPV-I Main Test Series (V31.2-V34)

L. Wolf

Projekt HDR-Sicherheitsprogramm, Kernforschungszentrum Karlsruhe GmbH, Postfach 3640, D-7500 Karlsruhe 1, Germany

SUMMARY

This paper summarizes the experimental results of the four blowdown tests (V31.2, V32, V33, V34) with reactor pressure vessel internals (RPV-I) constituting the Main Test Series at the HDR-facility. These experiments differ from the previously reported Preliminary Test Series [1] by a substantial increase in instrumentation and by covering a broader spectrum of important problems of fluid/structure interactions. The main objectives of the respective experiments were:

V31.2: replication of previous tests V31.0 and V31.1 [1]

V32:   German Standard Problem No. 5, higher loadings due to increased subcooling of the downcomer fluid

V33:   reduced loading due to small break conditions (0.25 F) at otherwise identical thermodynamically initial conditions as V32

V34:   isothermal test with the upper core barrel flange not rigidly clamped, allowing axial flange and radial core barrel lower end impacts against the pressure vessel.

The most important conclusions from the experimental data are:

1)   Increasing the subcooling to 78 °C in the downcomer (V32) results in increased local and global loads by about 15 % compared to V31.1 performed with 50 °C subcooling.

2)   The reduction of the break cross-sectional flow area down to 25 % (V33) of the full area (V32) results in reductions by 10 % to 40 % in loads and structural responses of the measured for V32.

3)   Axial and radial core barrel impact phenomena (V34) greatly change core barrel dynamics but barely affect fluid dynamics.

Additionally, an overview and first assessment are presented of the comparisons between the data and pre-test predictions with a variety of computer codes for the different experiments. Throughout this session, more detailed comparisons and code descriptions will be separately provided by various authors of German and American institutions participating in the HDR program.

Overall, the HDR-RPV-I experiments of the Main Test Phase have greatly extended the insight into more complex issues of FSI-phenomena, thereby contributing to ongoing changes in the licensing requirements concerning RPV-I loads in the FRG.

1. INTRODUCTION

After the results of the Preliminary Test Series (V29.2 - V31.1) had provided a first set of reliable data /1,2/ on fluid/structure interaction phenomena and the first verification loop of pre- and post-test predictions had been completed and resulted in satisfactory to very good agreements between data and calculations, it was decided to continue the experimental program of HDR-RPV-I tests with an additional set of four tests. In a order to comply with the changing environment of licensing requirements concerning RPV-I loads in the FRG the original set of tests was reformulated. Analytically, the time was used by some institutions to improve the predictive quality of their codes, performing additional post-test calculations, changing nodalizations, numerical schemes or extended the codes capabilities such as for instance FLUX-4 /3/ by including the structural dynamics response of the RPV and implementing non-linear structural impact phenomena. Especially the latter feature enabled the Project HDR to carefully design the special experiment, V34, by allowing the core barrel to move axially and radially impact at its lower end against the RPV.

This paper highlights some of the experimental findings and gives an overall review of the comparisons between the data and the multitude of pre-test calculations. More detailed descriptions of the individual codes and their verifications based upon the new data are provided by the various authors in the following presentations covering the whole spectrum of FSI-code methodology known thus far.

2. DESCRIPTION AND TEST MATRIX OF RPV-I EXPERIMENTS V31.2 - V34

Fig. 1 represents a cross-section of the HDR pressure vessel and the arrangement of the flexible core barrel together with same important overall measures. Steady-state enthalpy distributions in the various fluid regions are obtained by filling hot water into the upper and cold water into the lower plena. The core barrel carries a mass ring at its lower flange and is rigidly clamped at its upper flange for the experiments V31.2 thru V33. Some additional hardware changes had to be introduced in order to achieve the major objectives of tests V33 and V34. For V33, an orifice with only 25 % cross-sectional flow area was installed just upstream of the break disks in the break nozzle. For test V34, the upper flange is not rigidly clamped as in all other tests but allowed to move axially and somewhat radially. Also, snubbers as shown in the insert of Fig. 1 have been mounted at the mass ring for this test to reduce the radial clearance in order to ensure radial impact against the RPV. In order to closely follow the axial core barrel movement, three additional displacement sensors, distributed around the circumference of the upper core barrel flange, were added to the instrumentation plan.

Fig. 2 presents a flow sheet of the overall rationale behind the sequence of the various RPV-I tests performed at the HDR-facility, thus far. Experimental and analytical results for tests V29.2 through V31.1 have been already reported in /1,2/ as well as by a variety of institutions participating in the HDR-Safety Program. As indicated in Fig. 2, the four experiments can be characterized by the following objectives:

V31.2: Reproducibility of data, availability and reliability of sensors after a pause of a one year between V31.1 and V31.2

V32: Defined as German Standard Problem No. 5; load increase on core barrel by increase in subcooling in the downcomer by 28 °C compared to V31.2

B 6/1[*]

V33: Small break test; reduction in core barrel loads by decreasing the break flow cross-sectional area to 25 % of that of all other tests

V34: Effects of axial and radial core barrel impacts due to nonlinear structural boundary conditions with the additional simplification of isothermal conditions in the vessel

Fig. 3 summarizes the thermodynamic initial conditions just prior to blowdown initiations for the respective tests. The conditions for V31.2 replicate those of V31.0 and V31.1 of the Preliminary Test Series. For the three other tests the fluid subcooling in the downcomer has been kept at its maximum value of 78 °C which is achievable with the facility. In order to separate the effects of the break flow area reduction, tests V32 and V33 have been performed with identical initial conditions. On the other hand, to minimize any possible bypass effect at the loose upper core flange, isothermal conditions throughout the whole vessel were selected for V34. With the exception of the latter, axial temperature profiles in the core and to a lesser degree in the downcomer regions were established to simulate PWR conditions as closely as possible.

3. SUMMARY OF COMPUTER CODES USED FOR PRETEST PREDICTIONS

The computer codes used for pretest calculations fall into two main categories

a) codes accounting for fluid/structure interaction phenomena

b) codes which do not account for FSI phenomena by assuming a rigid core barrel

In what follows, only codes of category a) and their respective results will be discussed. Fig. 4 summarizes the codes, and compared to those introduced and discussed during the 6th SMIRT /1/, the additional entry of PISCES-3DELK (post-test calculation by BBR, Germany) is worth mentioning as well as the fact that K-FIX (3D, FLX) was used with implicit and explicit solution schemes by LANL and Battelle-Frankfurt, respectively. Thus, the breakdown of the number of pretest predictions with coupled codes with respect to the individual experiments reveals that

1) 8 American and German institutions participated with 7 different computer codes for test V32

2) 4 institutions predicted test V33

3) only IRE-KfK predicted V34 with FLUX4 /3/ (Two more post-test predictions are expected)

The details, main features, as well as the individual comparisons of experimental and calculational results of these codes are the subjects of the following representations of Session B6. The codes listed in Fig. 4 span the whole spectrum of modeling schemes known for coupled fluid/structure interactions. Numerically, the codes use widely different methods such as for instance the Method-of-Characteristics (3 codes), Implicit-Continuous Eulerian Approach (1 code), Langrangian-Eulerian Method with rezoning (2 codes) and fully implicit-analytical approach (1 code). Compared to the status as described in 1981, various extensions and improvements have been implemented into different codes and tested against the data of V31.1 with post-test calculations in order to approach the Standard Problem with optimized tools.

4. EXPERIMENTAL RESULTS

4.1 Fluiddynamic Quantities

In the following, the experimental data of all of the four experiments are superimposed in one figure for one sensor type and location in order to more easily comprehend similarities and deviations among the results of the tests.

Figs. 5 and 6 show the absolute pressures at the break and in the downcomer in the break nozzle axis, respectively.

1) The steep initial decompression rate is the same for all four experiments and obviously independent of the break size and fluid temperature under the conditions studied.

2) In all four experiments, the pressures at the break undershoot the saturation pressures thereby initializing a flashing process. The degree of undershoot depends upon the initial subcooling; an increase in subcooling (V32 vs. V31.2) increases the drop but decreases the difference between saturation and maximum undershoot pressure.

3) The pressure increase following the initial decompression heavily depends upon fluid subcooling (V31.2 vs. V32), and break size (V33 vs. V32, V31.2 and V34).

4) Restricting the break size by 75 % (V33 vs. all other tests) leads to a pressure recovery in the break nozzle close to the initial pressure level.

5) Increasing the subcooling (V32 vs. V31.2) leads to pronounced pressure wave effects upstream of the break location towards the pressure vessel because the extent of single phase flow is enlarged.

6) The initially steep decompression wave in the break nozzle is effectively damped once it reaches the three-dimensional downcomer region. Up to 5 ms the course of the transient is the same for all four tests. Whereas the pressure keeps decreasing for tests V31.2, V32 and V34, it starts recovering for V33 already for times larger than 5 ms.

7) The increase in subcooling (V32 vs. V31.2) has only minor effect upon the pressure history. Slightly lower pressure levels are reached throughout the first 145 ms. After that, the pressure recovers faster and reaches a higher pressure level than what is observed for V31.2. Obviously, the HDR-specific nonequilibrium effect in the core region and upper plenum is much more pronounced for increased subcooling. At t = 190 ms pressures of V32 and V33 approach each other.

8) The effect of isothermal condition (V34 vs. V32) takes effect starting at about 30 ms. Up to 100 ms both curves run in parallel; after that they deviate substantially.

Fig. 7 summarizes the pressure differences across the core barrel at the break nozzle axis and leads to the following conclusions:

1) The increase in subcooling by 50% results in an increase of the maximum pressure difference of only 15 %. Thus, the load increase for test V32 is fairly small.

2) Reducing the break size area by 75 % leads to a reduction of only 40% in the maximum pressure difference. The maximum pressure difference occurs only for a very brief time duration.

3) The comparisons for V32 and V34 show that the nonlinear effects in the structural boundary conditions and radial impacts in test V34 affect the loading history only at times larger 80 ms, after which the differential pressure oscillations are much faster damped than for V32. Essentially, there is no feedback of the nonlinearities in the boundary conditions (V34) upon the fluiddynamic loading throughout most of the early portions of

the transient.

4) Despite the variety of initial and boundary conditions of the three experiments, the major dynamic characteristics in the loading histories remain about the same.

4.2 STRUCTURAL QUANTITIES

Fig. 8 and 9 summarize the comparisons of the radial displacements at the upper and lower positions of the core barrel for all four experiments, respectively. From this evidence, the following conclusions can be drawn:

1) Generally, the amplitudes of the displacements show the same trends as those already discussed for the pressure difference. The dynamic behavior is about the same for all tests.

2) The increase in downcomer subcooling by 50 % increases the displacements by about 15 % independent of their positions.

3) The reduction in break size by 75 % (V33) results in a 35 % to 75 % reduction in the maximum displacement, dependent upon the position considered. Positions close to the break nozzle are much less affected by the break size than those further off.

4) Additional radial clearances at the upper flange seat (V34) leads to an increase of the maximum displacement by about 50 % at the top and bottom of the core barrel which thereby impacts the RPV both at 90° and 270°. In addition, the impact at the lower core barrel drastically changes the whole dynamic behavior of the displacements in this region by reducing the frequency of the core barrel movements by about a factor of 2. The courses of the displacement histories suggest direct contacts between core barrel and RPV for a prolonged time span. The results show that forces, strains, stresses and accelerations induced by impacts in addition to the depressurization transient are small.

Fig. 10 summarize the histories of the three axial displacement sensors following the axial uplifting of the core barrel in test V34. These results have not yet been corrected for disturbances introduced by the additional flexibility of the measurement system. It becomes obvious from these curves that the core barrel is lifted axially at 40 ms without any sideward tumbling once the pressure difference across the core barrel becomes positive, (compare Fig. 7), e.g. the pressure in the downcomer is larger than in the core region. The core barrel reseats at 80 ms. A second uplift starts around 105 ms and ends around 150 ms. A third follows. After that the CB is damped again due to clearance reduction of the seat as a result of system decompression.

The data of V34 provide a meaningful data basis for the effect of nonlinearities at a large scale facility on FSI phenomena for the first time.

5. COMPARISONS BETWEEN DATA AND PRETEST CALCULATIONS

The comparisons between experimental data and blind pretest predictions by the computer codes listed in Fig. 4 are performed on a test-by-test basis and only for the two quantities pressure difference, KP 9, and displacement, KS 1030, in what follows. For the sake of clarity in the graphical presentations, the results of both equivalent network codes DAISY and MULTIFLEX are shown together with those by FLEXWALL which uses a mixture of lumped and 2 1/2 D models. On the other hand, the results of all truely 3-D codes for the fluid regions inside the RPV are plotted together. Naturally, of foremost interest are the conclu-

sions which may be derived from the Standard Problem No. 5 (V32) comparisons. Without fore-
stalling any official comments on these issues, the following observations from Figs. 11
through 14 seem to be in order:

1) Both FLEXWALL and MULTIFLEX greatly overestimate the maximum pressure difference across
   the core barrel, as shown in Fig. 11 at the break nozzle axis. Whereas the latter consi-
   stently overpredicts, FLEXWALL results underestimate the following experimental extremes
   and depicts a rather large frequency shift. These deviations are substantially reduced
   for positions further off the break nozzle. Overall, the best agreement in this category
   of codes is obtained by DAISY which consistently matches both amplitudes and frequency
   very well thereby approaching the quality of the 3-D codes as shown in Fig. 12.

2) Fig. 12 impressively demonstrates the overall superiority and consistancy of the truely
   3-D codes because of their ability to achieve best-estimate results compared with the
   data seemingly independent of fluid and structural models used. Deviations, if any, are
   consistently on the conservative side. PISCES-3DELK shows the least satisfactory results
   in this category by substantially overpredicting the first extreme. Pronounced calcula-
   tional pressure wave phenomena do not match with the experimental observations. Calcula-
   tions by STEALTH/WHAMSE were also stopped at 85 ms, apparently because it was felt that
   the implemented fluid model would lead to inappropriate results beyond this point in
   time. Although the fully explicitely operated K-FIX (3D,FLX) (Battelle) develops large
   numerical fluctuations beyond 160 ms it continues the calculation despite of the obvious
   shortcoming of the solution scheme chosen for the prevailing two-phase situation. This
   special situation is much better handled by the implicitely run version (LANL) and the
   FLUX-DRIX combination (IRE-KfK).

3) Fig. 13 summarizes the results of the first category of codes for the displacement at
   the lower core barrel end. All major characteristics are met with more or less devia-
   tions compared to the data.

4) Fig. 14 compares the results of the best-estimate codes at the same position and shows a
   somewhat closer agreement of their results with the data. Worth mentioning though is the
   fact, that despite an extreme refinement in the nodalization, especially in the FLUX-co-
   de, the first displacement maximum is still somewhat underpredicted. This deficiency
   seems to be characteristic of all of these codes.

Figs. 15 through 18 show the same comparisons for the small break experiment V33. The follo-
wing conclusions can be drawn from the comparisons between the individual calculations and
the experimental data as well as between the two categories of codes:

1) Given the a priori unknown situation, the results of the blind pre-test predictions of
   all codes agree remarkably well with the data. However, it is interesting to note that
   all codes of the first category overpredict the first extreme by the same amount.

2) Again, given all circumstances, the best-estimate codes of the second category prove
   their superpriority in predictive quality under different conditions. In addition for
   V33 the previously observed deficiencies in calculating the displacements are eliminated.

3) Because no two-phase effects occur in the system during the time period considered, the
   fully explicit solution scheme in K-FIX (Battelle) proves adequate for a minimum in com-
   putation time.

The only pre-test predictions for the test V34 was performed by IRE-KfK with FLUX4.

B 6/1[*]

These, together with the post-test predictions will be highlighted in the following presentation by U. Schumann. Here, it should suffice to mention that fluiddynamic quantities, and strains were already well met by the pre-test predictions, because they did not vary dramatically from V32 for most of the time period considered here. The quality of the predicted radial displacements were inadequate but have been substantially improved since then, demonstrating the basic adequacy of the extension in the structural model for this code /3/.

Finally, it should be pointed out, that first comparisons between experimental and calculated stresses show reasonable agreement thereby adding yet another important dimension in the assessment process of FSI computer codes.

6. CONCLUSIONS

The Main Test Series V31.2 - V34 has enlarged the insight into the understanding and interpretation of FSI phenomena under a variety of different thermodynamic initial conditions as well as fluiddynamic and structural boundary conditions. By virtue of the enlarged test bed of data, the HDR test field of verification efforts for the RPV-I tests (see Fig. 2 of /2/) has been substantially broadened. This allowed the reevaluation of the predictive qualities of the various computer codes used for blind pre-test predictions for a variety of different loading histories. Not unexpectedly, the agreements between data and analytical results have substantially improved compared to those for the Preliminary Test Series /2/. This is certainly a result of the full feedback of the learning process concerning numerical schemes, modeling features and parameters, thereby confirming the philosophy of PHDR to go through a complete, well-orchestrated loop of comparisons between pre- and post-test calculational results with the experimental data.

The assessment of the first step in the second verification loop on the basis of the results of the Main Test Series indicates a very satisfactory agreement with the analytical predictions showing a maximum deviations of $\pm$ 15 % compared with the measured data (pressure difference, displacements, strains). Only few of the codes fall outside this region. However, in nearly all instances the observed deviations lie on the conservative side. The associated increase in the confidence of both the experimental data as well as the computer codes should have impacts upon practical implications in design and licensing. Although the differences between the results of the various computer codes have been substantially decreased, best-estimate codes still show certain superpriorities.

REFERENCES

/1/ WOLF, L., SCHUMANN, U., SCHOLL, K.-H., "Experimental and Analytical Results of Coupled Fluid-Structure Interactions During Blowdown of the HDR-Vessel", Proceedings Sixth Intl. Conf. on Structural Mechanics in Reactor Technology, Paris, France, Aug. 17-21, 1981, Paper B2/1*

/2/ WOLF, L., "Experimental Results of Coupled Fluid-Structure Interactions During Blowdown of the HDR-Vessel and Comparisons With Pre- and Post-Test Predictions", Nucl. Eng. Design 70, 269-308 (1982)

/3/ SCHUMANN, U., "Experimental and Computed Results for Fluid-Structure Interactions With Impacts in the HDR-Blowdown Experiment", Nucl. Eng. Design (1983) in press
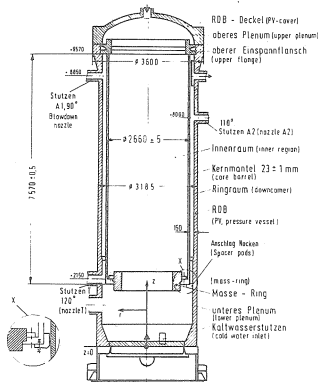
Fig. 1.　HDR Reactor Pressure Vessel and Core Barrel

Fig. 2.　Sequence of Tests

TEST No	Pressure bar	Upper Core Temp. °C	Downcomer Temperature °C	Subcooling Downcomer Degrees	Length of break nozzle m
V 31.2	110	308	268	50	1.369
V 32	110	308	240	78	1.369
V 33	110	308	240	78	1.369
V 34	110	240	240	78	1.369

Fig. 3.　Test Matrix
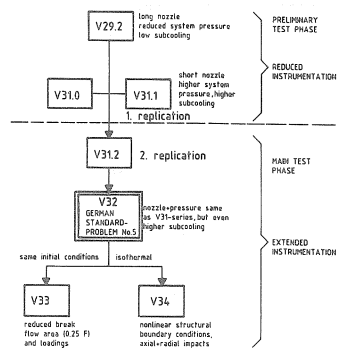
CORE ABBREVIATION	CODE NAME	INSTITUTION COUNTRY	REMARKS
DAI	DAISY	GRS, GERMANY	COUPLED NETWORK
EZMA	EXPERIMENTAL DATA	PHDR, GERMANY	COUPLED
FLE	FLFXM/ALL	KWU, GERMANY	COUPLED; 2 1/2 D DOWNCOMER, LECK BREAK NOZZLE AND CORE REPRESENTATION
FDS	FLUX-DRIX	IRE-KfK, GERMANY	COUPLED; WITH PRESSURE BOUNDARY CALCULATED AT NOZZLE INLET BY DRIX, STRONG COUPLING BETWEEN BOTH CODES
FDW	FLUX-DRIX	IRE-KfK, GERMANY	SAME AS ABOVE, BUT WEAK COUPLING BETWEEN BOTH CODES
KFXL	K-FIX(3D,FLY)	LANL, USA	COUPLED; FULLY IMPLICIT SOLUTION
KFXB	K-FIX(3D,FLY)	BATTELLE FRANKFURT, GERMANY	COUPLED; FULLY EXPLICIT
MFX	MULTIFLEX	W, USA	COUPLED NETWORK
STE	STEALTH/WAMSE	EPRI, SAI, ITI,	COUPLED; LAGRANGE-EULER, REZONING
PISC	PISCES-BRELK	PRB, GERMANY	COUPLED; LAGRANGE-EULER

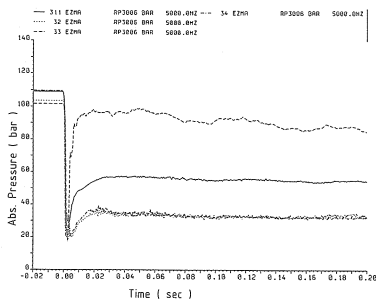Fig. 4.　Computer Codes

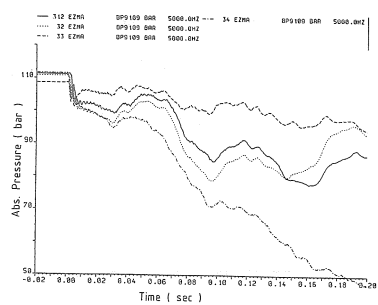Fig. 5.　Pressures at Break

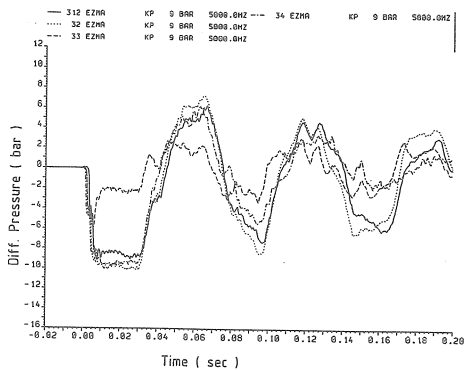Fig. 6.　Pressures in Downcomer at Break Nozzle

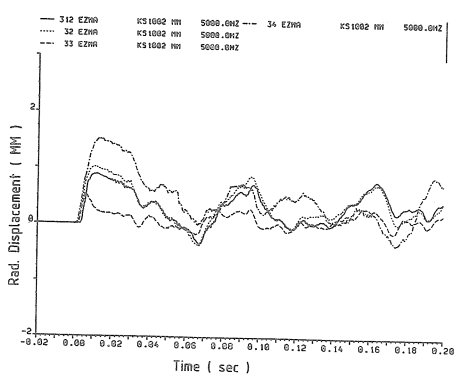Fig. 7.   Pressure Differences at Break Nozzle

Fig. 8.   Radial Displacements Above Break Nozzle
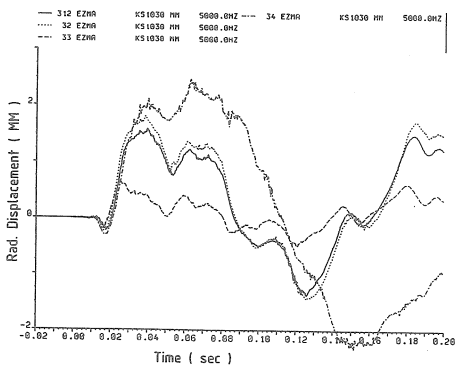

Fig. 9.   Radial Displacements at Lower CB End
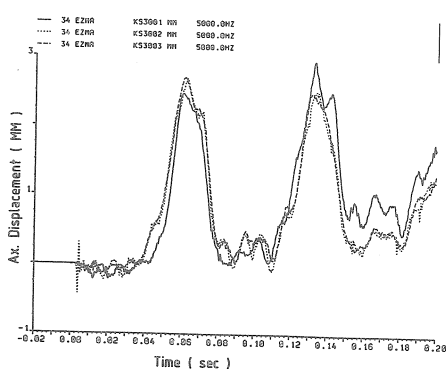

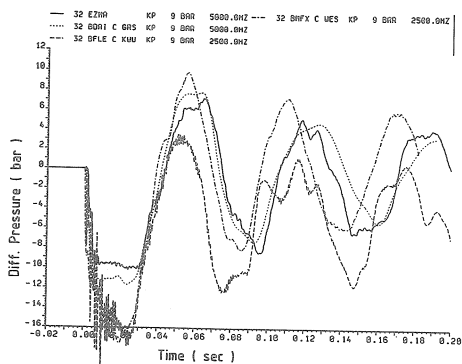Fig. 10.   Axial Displacements at Upper CB Flange

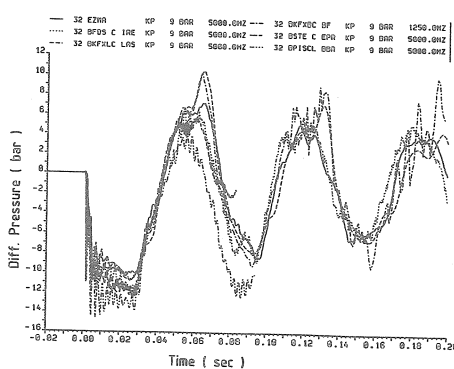Fig. 11.   V32: Comparisons Pressure Differences; Network Codes

Fig. 12.   V32: Comparisons Pressure Differences; Best-Estimate Codes

Fig. 13. V32: Comparisons Displacements;
Network Codes

Fig. 14. V32: Comparisons Displacements;
Best-Estimate Codes

Fig. 15. V33: Comparisons Pressure
Differences; Network Codes

Fig. 16. V33: Comparisons Pressure Differences;
Best-Estimate Codes

Fig. 17. V33: Comparisons Displacements;
Network Codes

Fig. 18. V33: Comparisons Displacements;
Best-Estimate Codes